Covalency driven low-temperature structural distortion and its effect on electronic structure of $Hg_2Ru_2O_7$

Santu Baidya and T. Saha-Dasgupta

Department of Condensed Matter Physics and Materials Science, S. N. Bose National Center for Basic Sciences, JD-III, Salt Lake City, Kolkata 700098, India

(Received 21 October 2014; revised manuscript received 28 December 2014; published 23 February 2015)

We investigate theoretically the possible low temperature structural distortion in the pyrochlore based ruthenate compound $Hg_2Ru_2O_7$. Our study reveals a signature of structural distortion leading to charge disproportionation between the Ru ions in the unit cell. The charge disproportion is found to be driven by the energy gain due to large covalency originating from the overlap of extended Ru 5*d* and O 2p orbitals combined with Hg *d*-Ru *d* hybridization. The exchange interaction operative between the charge disproportionated Ru ions turns out to be of antiferromagnetic nature, which drives the insulating state and stabilizes the noncollinear magnetic structure. Our study sheds light on the microscopic mechanism of the low temperature structural transition in this compound.

DOI: 10.1103/PhysRevB.91.075123 PACS number(s): 71.30.+h, 71.20.−b, 71.15.Mb

I. INTRODUCTION

Pyrochlore compounds containing 3*d* transition metal (TM) ions have attracted attention for a long time due to the unconventional properties exhibited by them including the strong frustration effect [1]. Pyrochlore oxides with TM ions from the 4*d* series add another dimension to the topic, as the 4*d* electrons are expected to be at the borderline between localized and itinerant electron behavior. A wide variety of 4*d* TM based pyrochlore oxides have been synthesized, among which $A_2^{3+}Ru_2^{4+}O_7$ compounds with Ru^{4+} valence have been studied most extensively, e.g., $Y_2Ru_2O_7$ [2], $Bi_2Ru_2O_7$ [3], $Tl_2Ru_2O_7$ [4], $Pb_2Ru_2O_7$ [5], and $Ln_2Ru_2O_7$ with Ln = Pr-Lu [6]. On the other hand, only a handful of Ru-based pyrochlore oxides with highly uncommon oxidation state of Ru^{5+} valence have been synthesized. The only known examples are $Cd_2Ru_2O_7$, $Ca_2Ru_2O_7$ [7], and $Hg_2Ru_2O_7$ [8]. While the properties of $Cd_2Ru_2O_7$ and $Ca_2Ru_2O_7$ have not been explored in detail, detailed study of the properties of $Hg_2Ru_2O_7$ (HRO) have been carried out. A well defined metal-insulator transition (MIT) was reported at ≈107 K, with an order of magnitude jump in the resistivity ρ, and insulating temperature dependence of resistivity at temperatures below 107 K [9]. This phenomena is in striking similarity with the first-order MIT reported for $Tl_2Ru_2O_7$ [4]. $Tl_2Ru_2O_7$ shows a MIT at ≈125 K, accompanied by a structural phase transition from cubic to orthorhombic structure. It thus appears at first sight that the $Tl_2Ru_2O_7$ with Ru^{4+} ions and $Hg_2Ru_2O_7$ with Ru^{5+} ions behave similarly. However, it is to be noted that Ru^{4+} ion in $Tl_2Ru_2O_7$ is in d^4 state, which in low spin (LS) configuration of $S = 1$ with t_{2g}^4 occupancy is orbitally active. The MIT in $Tl_2Ru_2O_7$ was argued to be driven by formation of one-dimensional Haldane chains due to orbital ordering of localized Ru 4*d* electrons [10]. Ru^{5+} ion in $Hg_2Ru_2O_7$ in $S = 3/2$ state with t_{2g}^3 configuration, on the other hand, is not orbitally active. The nuclear magnetic resonance (NMR) measurement [11] reported a significantly smaller moment of Ru for $Hg_2Ru_2O_7$ than expected out of nominal valence of Ru^{5+} and a magnetically ordered state at low temperature (LT) instead of spin-singlet ground state as in $Tl_2Ru_2O_7$, suggesting the nature of Ru 4*d* electronic wave function in the two compounds to be different, and the MIT's having different origins. Recent density functional theory (DFT) supplemented with Coulomb *U* study [12] finds that for the choice of same Coulomb *U* value, while the Ru magnetic moment in $Tl_2Ru_2O_7$ attains the fully polarized value of 2 μ_B, Ru magnetic moment in $Hg_2Ru_2O_7$ is far smaller compared to 3 μ_B. This points towards more itinerant character of Ru electrons in $Hg_2Ru_2O_7$, compared to that in $Tl_2Ru_2O_7$, which was explained [12] to arise from much stronger Hg *d*- Ru *d* covalency, compared to small Tl *d*-Ru *d* covalency.

Both ρ(T) and the temperature dependence of susceptibility, χ, in $Hg_2Ru_2O_7$ were found to show hysteresis, suggesting the first-order nature of the MIT. The first order nature of the transition implies a structural phase transition associated with the MIT. The NMR data also hints towards the structural phase transition together with the stabilization of long range magnetic order at the transition temperature. The pertinent question in this context is, what drives the structural transition? While for $Tl_2Ru_2O_7$, it is due to orbital ordering driven formation of Haldane chains, the origin of structural transition for $Hg_2Ru_2O_7$ is not clear. The low temperature crystal structure has not been resolved until very recently. The low temperature crystal structure has been investigated by Duijn *et al.* [13] by high-resolution neutron powder diffraction. Rietveld refinement of the data showed two possible low temperature symmetries, orthorhombic and monoclinic, with a somewhat better fit for the monoclinic symmetry. The orthorhombic symmetry which allows for splitting of Ru sites in two inequivalent sites with ratio 1:1 is also inconsistent with NMR observations [11]. In parallel, characterization of the low temperature structure was undertaken in the group of Takagi *et al.* [14] which proposed the trigonal symmetry for the low temperature structure. In the present study, using the first-principles DFT based calculations, we investigate the structural and electronic properties of the low temperature phase. Our findings are summarized as follows, i) the DFT structural optimization shows the presence of two different RuO_6 octahedral volumes, considering any one of the two proposed symmetry of the low-temperature structures, monoclinic or trigonal. The very similar structural distortion obtained assuming either of the two proposed symmetries, monoclinic or trigonal, proves the obtained trend to be

robust. This provides clear signature of charge disproportionation in the system, reflected in its electronic properties like magnetic moments. Our study is expected to motivate further experimental investigation in the characterization of the low temperature structure and properties in light of the charge disproportionation effect. ii) the strong covalency effect discovered in the study of high temperature phase in our previous paper [12] is found to be the responsible factor in creating the charge disproportionated situation.

The finding of charge disproportionation offers a natural means to overcome the unusual valency of Ru5+. This, for example, is very similar in spirit to the case of $CaFeO_3$, in which the unusual Fe 4+ valency is avoided by charge disproportionation [15] to Fe $(4-\delta)+$ and Fe$(4+\delta)+$, but happening in $4d$ TM based oxide in the present case. Interestingly, the strong Fe-O covalency effect was argued to be the responsible factor for the charge ordering in the case of $CaFeO_3$ [16]. This leads us to the conclusion that the structural transition is triggered by the charge disproportionation and charge ordering transition, which concomitantly happens with the MIT transition assisted by the antiferromagnetic coupling between the Ru ions.

II. METHODOLOGY

The calculations have been carried out in three choices of basis sets: (a) full-potential linearized augmented plane-wave (FLAPW) calculations as implemented [17] in WIEN2k (b) plane wave based pseudo potential method within Vienna *ab initio* simulation package (VASP) [18], and (c) muffin tin orbital (MTO) based linear muffin tin orbital (LMTO) [19] and nth order MTO (NMTO) method [20]. The plane wave calculations have been used for efficient determination of the equilibrium structures as well as for calculation of electronic and magnetic properties. The results have been cross checked employing all electron method of FLAPW which makes no shape approximation to the potential. The LMTO/NMTO methods have been used to calculate the effective Wannier functions and the hopping interactions and effective energy levels. The reliability of the calculations in different basis sets has been established in terms of comparison of band structure and density of states.

For FLAPW calculations, we chose the APW + lo as the basis set and the expansion in spherical harmonics for the radial wave functions was taken up to $l = 10$. The charge densities and potentials were represented by spherical harmonics up to $l = 6$. For Brillouin zone (BZ) integration, we typically considered about 200 k points in the irreducible BZ and modified tetrahedron method was applied [21]. The commonly used criterion for the convergence of basis sets relating the plane wave cutoff, K_{max}, and the smallest atomic sphere radius, R_{MT}, R_{MT}*K_{max}, was chosen to be 7.0. For the plane wave calculation, we have used projected augmented wave (PAW) potentials [22] and the kinetic energy cutoff for expansion of wave functions used was 500 eV. Reciprocal space integrations have been carried out with a k space mesh of $8 \times 8 \times 8$. The valence electron configurations for the compounds were chosen as Hg/Tl $6s6p5d$, Ru $5s5p4d$, and O $2s2p$. The applied exchange-correlation functional was chosen to be the generalized gradient approximation in the Perdew, Burke, and Ernzerhof (PBE) parametrization [23]. In order to take into account the improved treatment of the missing correlation beyond GGA, we have carried out GGA + U calculations [24]. The U value at Ru site is chosen to vary between 1 and 3 eV, with Hund's coupling parameter J_H fixed at 0.7 eV. The qualitative trend in the obtained results are found to be independent of the choice of U value within the specified window. The results presented in the following are obtained with a U value of 2 eV. We have also carried out a calculation including spin-orbit coupling. The basic conclusions are found to remain unaltered. The orbital moment at Ru site is found to be tiny with a value of 0.04–0.07 μ_B, depending on the choice of U value and the different symmetries. NMTO calculation, which is yet to be made self consistent, relies on potential parameters borrowed from LMTO. In the LMTO calculation, the radii of the MT spheres at Hg, Ru, and O sites were chosen to be about 1.5 Å, 1.3 Å, and 1.0 Å, respectively. The space filling was achieved with 5, 5, and 3 different empty spheres in the low-temperature trigonal, monoclinic, and high-temperature cubic structures, respectively.

III. LOW TEMPERATURE CRYSTAL STRUCTURE - STRUCTURAL OPTIMIZATION

Among the two proposed low temperature crystal structures, one is of monoclinic symmetry in $C2/m$ space group and another is of trigonal symmetry in $R\bar{3}m$ space group. The lowering of symmetry from the cubic $Fd\bar{3}m$ space group to monoclinic $C2/m$ space group splits the Ru site of multiplicity 4 into three inequivalent Ru sites (Ru1, Ru2, Ru3) of multiplicities 2, 1, and 1. Similar splitting occurs at Hg and O sites resulting into three inequivalent Hg sites (Hg1, Hg2, Hg3) and five inequivalent O (O1, O2, O3, O4, and O5) atoms. The trigonal space group, on the other hand, allows for two inequivalent Ru sites (Ru1, Ru2), two inequivalent Hg sites (Hg1, Hg2), and three inequivalent O sites (O1, O2, and O3). The different Wyckoff positions of atoms in the proposed low symmetry structures, in comparison to that of the high temperature (HT) cubic structure, are listed in Table I. We find since the Ru and Hg sites occupy the high

TABLE I. The Wyckoff positions and multiplicity of different atoms listed for the high temperature cubic $Fd\bar{3}m$ symmetry, low temperature trigonal $R\bar{3}m$ symmetry and low temperature monoclinic $C2/m$ symmetry.

$Fd\bar{3}m$			$R\bar{3}m$			$C2/m$		
	Mult.	Wyc.		Mult.	Wyc.		Mult.	Wyc.
Hg	4	d	Hg1	3	e	Hg1	2	f
Ru	4	c	Hg2	1	b	Hg2	1	d
O	12	f	Ru1	3	d	Hg3	1	b
O′	2	b	Ru2	1	a	Ru1	2	e
			O1	2	c	Ru2	1	a
			O2	6	h	Ru3	1	c
			O3	6	h	O1	4	j
						O2	4	j
						O3	2	i
						O4	2	i
						O5	2	i

TABLE II. Optimized crystal structure of low temperature monoclinic and trigonal phase of $Hg_2Ru_2O_7$.

space group = $R\bar{3}m$, a = 7.189 Å, c = 17.638 Å				space group = $C2/m$, a = 12.465 Å, b = 7.206 Å, c = 7.210 Å			
Atoms	x	y	z	Atoms	x	y	z
Hg1	− 0.3333	− 0.1667	0.3333	Hg1	0.2500	0.2500	0.5000
Hg2	0.0000	0.0000	0.5000	Hg2	0.0000	0.5000	0.5000
Ru1	0.3333	0.1667	0.1667	Hg3	0.0000	0.5000	0.0000
Ru2	0.0000	0.0000	0.0000	Ru1	0.2500	0.2500	0.0000
O1	0.0000	0.0000	0.6257	Ru2	0.0000	0.0000	0.0000
O2	0.4100	0.2050	0.2721	Ru3	0.0000	0.0000	0.5000
O3	0.2026	0.4052	0.4740	O1	− 0.1254	− 0.1925	0.3163
				O2	0.3727	0.6958	− 0.0778
				O3	0.0671	0.0000	0.3164
				O4	− 0.3230	0.0000	− 0.0774
				O5	0.6256	0.0000	0.3768

symmetry positions, the free coordinates are only associated with oxygen positions. We carried out structural optimization where the atomic positions have been completely relaxed maintaining the space group constraint, starting from the experimental estimates as initial guess values until the forces became less 0.01 eV/Å. With Hg and Ru atoms occupying the high symmetry positions, the changes in atomic coordinates happen only for oxygen atoms, and in the free coordinates. Table II lists the lattice constants as well as atomic positions in the optimized structure in trigonal as well as monoclinic symmetry. The shifts of the free coordinates in the optimized structure from the initial guess values are shown in Fig. 1. We find the shifts to be significant, with important bearing on the structures, as described in the following.

The most important outcome of the structural optimization is that concerning the RuO_6 octahedral volumes and the octahedral distortions. For the experimental crystal structure in monoclinic symmetry, the volumes of the three equivalent

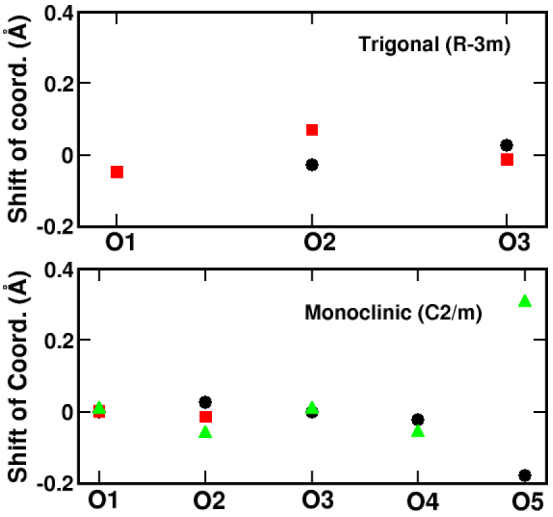

FIG. 1. (Color online) The shift in optimized atomic coordinates from the initial guess values. Shown are only those corresponding to free coordinates, which for O1, O2, and O3 in trigonal symmetry are x (circle) and y (square), for O1 and O2 in monoclinic symmetry are x (circle), y (square) and z (triangle), for O3, O4 and O5 in monoclinic symmetry are x (circle) and z (triangle).

RuO_6 octahedra, $Ru1O_6$, $Ru2O_6$, and $Ru3O_6$ are found to be the same which have six equal Ru-O bond lengths and a trigonal distortion making O-Ru-O bond angle different from 90°. For the experimental crystal structure in trigonal symmetry, the volumes of the two inequivalent RuO_6 octahedra are significantly different, with a volume difference, $V(Ru1O_6) - V(Ru2O_6) = 1.124$ Å^3. The $Ru2O_6$ octahedra is regular with equal Ru-O bond lengths and $Ru1O_6$ octahedra is Jahn-Teller distorted and compressed with compression in Ru-O bond length of 0.05 Å. Upon structural relaxation, the theoretically optimized structures show rather an interesting

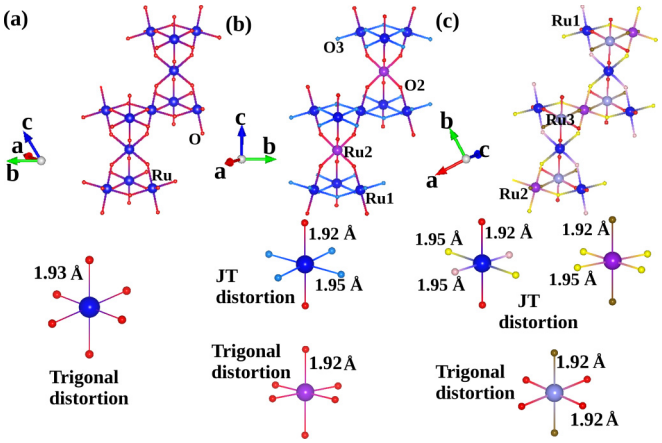

FIG. 2. (Color online) Optimized crystal structures of $Hg_2Ru_2O_7$ for HT cubic [panel (a)], LT trigonal [panel (b)], and LT monoclinic [panel (c)] structures. The upper panels show the connected Ru-O network, while the lower panels show the inequivalent RuO_6 octahedra. The large and small balls represent Ru and O atoms, respectively. The cubic structure contains only one type of RuO_6 octahedra with uniform Ru-O bond lengths, but with trigonal distortion of O-Ru-O angle deviating from 90°. The trigonal structure contains two inequivalent Ru atoms, Ru1 and Ru2. $Ru2O_6$ octahedra have uniform Ru-O bond lengths, but with trigonal distortion, while $Ru1O_6$ octahedra in addition to trigonal distortion has Jahn-Teller-like distortion with unequal bond lengths. The monoclinic structure contains three inequivalent Ru atoms, Ru1, Ru2, and Ru3. $Ru3O_6$ octahedra have uniform Ru-O bond lengths, but with trigonal distortion, while $Ru1O_6$ and $Ru2O_6$ octahedra in addition to trigonal distortion, has Jahn-Teller-like distortion with unequal bond lengths.

TABLE III. The bond lengths, bond angles, and octahedral volumes after the relaxation of ionic position coordinates for high temperature cubic symmetry, low temperature trigonal symmetry, and low temperature monoclinic symmetry.

	$Fd\bar{3}m$		$R\bar{3}m$		$C2/m$	
Bond length (Å)	Ru-O × 6	1.93	Ru1-O2 × 2	1.92	Ru1-O1 × 2	1.92
			Ru1-O3 × 4	1.95	Ru1-O2 × 2	1.95
			Ru2-O2 × 6	1.92	Ru1-O4 × 2	1.95
					Ru2-O2 × 4	1.95
					Ru2-O3 × 2	1.92
					Ru3-O2 × 2	1.92
					Ru3-O1 × 4	1.92
Bond Angle	∠ Ru-O-Ru	136.2°	∠ Ru1-O2-Ru2	138°	∠ Ru1-O1-Ru3	138°
			∠ Ru1-O3-Ru1	135°	∠ Ru1-O2-Ru2	135°
					∠ Ru2-O3-Ru3	138°
					∠ Ru1-O4-Ru1	135°
Vol	RuO_6 (Å^3)	9.62	$Ru1O_6$ (Å^3)	9.65	$Ru1O_6$ (Å^3)	9.69
			$Ru2O_6$ (Å^3)	9.55	$Ru2O_6$ (Å^3)	9.69
					$Ru3O_6$ (Å^3)	9.60

trend. For the monoclinic structure, $Ru1O_6$ and $Ru2O_6$ turn out to be compressed with Ru-O bond length difference of 0.03 Å, while the $Ru3O_6$ remains regular with equal Ru-O bond length. Although the initial guess had $Ru1O_6$, $Ru2O_6$, and $Ru3O_6$ octahedra of equal volumes, the structural optimization resulted into volume difference between $Ru1O_6$, $Ru2O_6$, and that of $Ru3O_6$, with $[V(Ru1O_6) = V(Ru2O_6)] - V(Ru3O_6) = 0.09$ Å^3. Rather surprisingly, the structural optimization carried out on trigonal symmetry structure resulted in $V(Ru1O_6) - V(Ru2O_6) = 0.10$ Å^3, significantly reduced compared to initial experimental guess, but in rather good agreement with the optimized monoclinic structure. The Ru-O bond length difference of 0.03 Å in the compressed $Ru1O_6$ octahedra, also agree with that in $Ru1O_6$ and $Ru2O_6$ octahedra in monoclinic structure, keeping the $Ru2O_6$ octahedra with uniform Ru-O bond length as in the case of $Ru3O_6$ octahedra in the monoclinic structure. Figure 2 shows the optimized crystal structures for the high temperature cubic, and low temperature monoclinic and trigonal structures. Various bond lengths and bond angles in the optimized structures are given in Table III.

The RuO_6 volume difference indicates structural signature of charge disproportionation between different inequivalent Ru's in the low temperature structure, which we investigate in the following. Interestingly, the RuO_6 volume difference is obtained in both trigonal and monoclinic symmetry, suggesting the observed presence of two different RuO_6 octahedral volumes to be a robust result. The comparison of the energies of the optimized low temperature structures shows trigonal symmetry structure to be lower in energy compared to that of the monoclinic structure by about 50 meV per formula unit. This is a small energy difference, especially considering the fact that it is $T = 0$ K estimate. Variation of U value between 1 and 4 eV is found to keep the magnitude of the energy difference more or less constant, with a variation of less than 3%. Increasing the U value beyond 5 eV or more, this energy difference is found to decrease. For a 4d Ru ion, a U value between 2–3 eV is believed to be a reasonable estimate. In the following the results have been presented for the optimized structure with trigonal symmetry. Similar calculations assuming the optimized monoclinic structure resulted in qualitatively very similar results, stressing the important influence of the presence of two different RuO_6 octahedral volume in the electronic structure, irrespective of the assumed monoclinic or trigonal symmetry.

IV. ELECTRONIC STRUCTURE OF LOW-TEMPERATURE STRUCTURE - SIGNATURE OF CHARGE DISPROPORTIONATION

The self-consistent electronic structure calculations in spin-polarized GGA + U set-up is found to converge to a solution with antiparallel alignment of Ru1 and Ru2 spins,

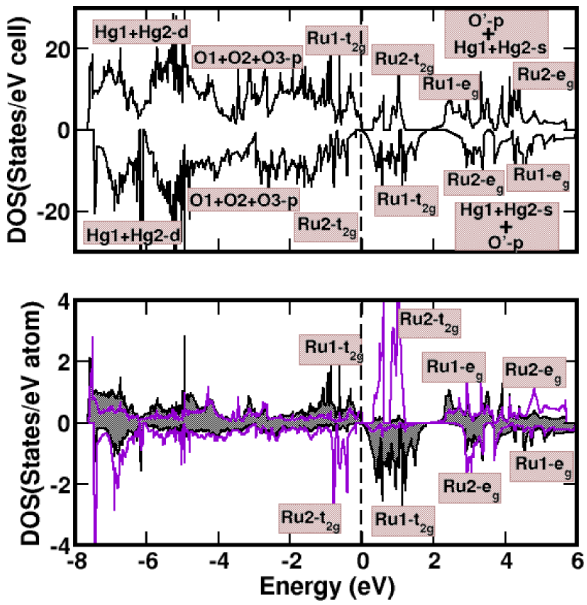

FIG. 3. (Color online) The total (upper panel) and partial (lower panel) density of states projected onto Ru1 d and Ru2 d sites in low-temperature trigonal structure. Marked are the dominant contributions of the states. The zero of the energy is marked at GGA + U Fermi energy.

TABLE IV. The ions with multiplicity and magnetic moment calculated as given in GGA + U calculation for the optimized low temperature trigonal symmetry ($R\bar{3}m$) structure.

	LT ($R\bar{3}m$)	
Ion	Multiplicity	Moment (μ_B)
Hg1	3	0.03
Hg2	1	0.06
Ru1	3	1.89
Ru2	1	− 1.63
O1	2	0.10
O2	6	0.05
O3	6	0.18

supporting the dominance of antiferromagnetic interaction, as concluded from the NMR experiment. The fixed moment calculation shows the antiparallel alignment to be energetically favorable over ferromagnetic alignment of Ru spins by about 20 meV/Ru. The computed total density of states and that projected to Ru1 d and Ru2 d states, considering the antiparallel alignment of Ru1 and Ru2 spins, are shown in upper and lower panels of Fig. 3, respectively. The Ru d-O p-Hg sd hybridized states are found to span an energy range of 8 eV below the Fermi level (E_F) to 6 eV above E_F. The states close to E_F are dominated by Ru t_{2g} states, with Ru e_g states being empty. The solution is found to be insulating with a small gap. As expected, increasing the U value increases the gap. The site projected d states at Ru1 and Ru2 sites appear to be rather different, indicating a difference in electronic structure between the two. Table IV shows the computed magnetic moments at various atomic sites. We find significant magnetic moment at O sites, stressing the importance of covalency in this compound. The moment at O2 site is relatively small which is shared between Ru1 and Ru2. The antiparallel alignment of Ru1 and Ru2 partly cancels the moment at shared oxygen site. The noticeable feature is the difference in magnetic moment between the Ru sites, which suggests different electronic occupancy of the two Ru sites. This is also reflected in the plot of the magnetization density, shown in Fig. 4, which shows a marked difference in magnetization density profile between Ru1 and Ru2. We further computed the energy level positions of the Ru1 and Ru2 t_{2g} states and the mean level position (averaging over the splitting arising due to Jahn-Teller as well as trigonal distortions in the octahedra) for Ru1 is found to be about 0.1 eV lower compared to Ru2, supporting a charge flow from Ru2 to Ru1. We note that the calculated charges at Ru sites using Bader's surface construction [25], shows 0.1 e^- charge difference between Ru1 and Ru2, with larger charge at the Ru1 site. Though the trend is in the right direction, the magnitude of the charge difference is small. Such small charge differences between differing charge states have been reported for doped manganites [26], TM impurities in semiconductors [27], and nickelates [28]. The strong covalency effect in case of HRO masks the charge disproportionation even further.

V. STABILIZATION MECHANISM FOR CHARGE DISPROPORTIONATION

Consideration of the d^{5+} nominal valence of Ru in HT and the splitting of 4 Ru sites in HT to 3 Ru1 and 1 Ru2 in

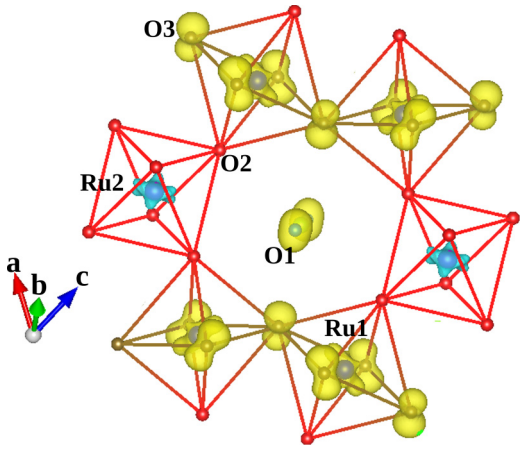

FIG. 4. (Color online) The distribution of magnetization density within the connected Ru-O octahedral ring, through which the rod shaped Hg-O structure passes. The yellow and cyan colors represent two different signs of the magnetization density. The signs of magnetization density located at Ru1 and Ru2 sites are opposite due to the antiparallel alignment of Ru1 and Ru2 spins. Significant magnetization densities are observed at O sites indicating the strong covalency effect.

LT, would advocate 4 × Ru d^{5+} ($e_g^{\pi}(\uparrow\uparrow)$ $a_{1g}(\uparrow)$) → Ru2 d^{6+} (e_g^{π} $(\uparrow\uparrow)$) + 3× Ru1 $d^{4.67+}$ ($e_g^{\pi}(\uparrow\uparrow)$ $a_{1g}(\uparrow)$ $e_g^{\pi}(\downarrow_{1/3})$) charge disproportionation scenario taking into account the a_{1g}-e_g^{π} trigonal crystal field splitting within the t_{2g} block of Ru d states. The computed magnetic moments as well as the electronic structure are far from this ideal picture indicating the charge disproportionation to be only partial, with Ru2 in $d^{(5+\delta)+}$ state and Ru1 to be in $d^{(5-\delta/3)+}$ state, with δ much smaller than 1, as found in the case of systems with large covalency. To shed light on the mechanism of charge disproportionation, we calculated the possible hybridization energy gain in LT phase compared to the HT phase. The effective Ru-O hybridization energy, as discussed in Ref. [29], can be defined as $h = \sum_{\sigma} \sum_{m=nn} \sum_{i,j=1}^{3} \frac{(t_{p_i d_j}^{m,\sigma})^2}{|\epsilon_{p_i,\sigma} - \epsilon_{d_j,\sigma}|}$, where the summation runs over the two spin channels, the six nearest neighbor Ru-O's and the over three p orbitals of oxygen and three t_{2g} orbitals of Ru. Muffin-tin orbital based NMTO-downfolding calculations were carried out, starting from the self-consistent GGA + U potentials as computed by LMTO, to have a first-principles estimate of $t_{p_i d_j}^{m,\sigma}$'s, $\epsilon_{p_i,\sigma}$ and $\epsilon_{d_j,\sigma}$. For this purpose, a Ru t_{2g}-O p Hamiltonian was constructed in the Ru t_{2g}-O p Wannier function basis, by integrating out degrees of freedom other than Ru t_{2g} and O p. We note that such a procedure takes into account the renormalization effect arising due to Hg d-Ru d covalency, on top of intrinsic Ru d-O p covalency. The onsite and off-site element in the two spin channels of the constructed Hamiltonian, as listed in Table VI, provides the estimates of ϵ-s and t's respectively. We find while the hoppings are rather similar in the two spin channels, the onsite energies are markedly different due to the spin splitting at Ru site. Plugging in the inputs from NMTO-downfolding calculations, $h_{Ru O_6}$(HT) turned out to be 3.29 eV, with $h_{Ru1 O_6}$(LT) = 2.90 eV and $h_{Ru2 O_6}$(LT) = 4.58 eV. This gives $3 \times h_{Ru1 O_6}$(LT) + $h_{Ru2 O_6}$(LT) > $4 \times h_{Ru O_6}$(HT)

with a net gain of about 0.12 eV. In order to obtain an alternative estimate, we have also calculated the quantity, $\int_{-\infty}^{E_f} n_d(E) \times n_p(E) dE$, for both the HT and the LT phases, where $n_d(E)$ and $n_p(E)$ are Ru d and O p projected partial density of states, as obtained in spin-polarized GGA + U calculation. This gave rise to a gain of 0.18 eV in LT phase compared to HT phase.

We note here, ideally the hybridization energy gain should have been calculated in the absence of magnetism. We found the charge disproportionation to be vanishing small for choice of $U = 0$ eV. All calculations therefore have been carried out in GGA + U set-up for choice of U values between 1 to 3 eV. The calculation set-up of GGA + U necessarily needs to include the spin polarization. To compare the LT and HT phases, both calculations were carried out assuming the same magnetic ordering in two phases, namely the antiparallel alignment of Ru spins. This is expected to cancel out the effect of magnetic ordering, leaving only the information of difference of the hybridization energy in two phases. This is supported by the fact that the estimate of hybridization energy gain turned out to be rather similar in calculations with choice of U values over window of 1 to 3 eV.

The hybridization energy gain, however, needs to be balanced by the restoring forces, which is given by the elastic energy associated with compression and expansion of the $Ru2O_6$ and $Ru1O_6$ octahedra, respectively, at LT compared to the uniform RuO_6 octahedra at HT. The elastic energy, for small displacements, is expected to be given by $\approx \frac{ku^2}{2}$, k being the stiffness constant. The first-principles estimate of elastic constants can be obtained from the DFT total energy as well as from forces acting on Ru ions as a function of small variation in Ru-O bond length from the equilibrium bond length. We carried out both the calculations. For the total energy calculation, the fitting function to extract the elastic constant was chosen as $f(u) = \frac{ku^2}{2} + cu^4$, while for the force calculation, the calculated data points were fitted with the function $-f'(u) = -ku - 4cu^3$. The variation of the energy and the force with variation in Ru-O bond length is shown in Fig. 5. This shows the stiffness of the lattice to be rather similar between the HT and LT, with estimates of $k = 28.20$ (28.25) eV/Å^2 and 25.56 (25.27) eV/Å^2 at LT and HT from total energy (force) calculation. The estimates of higher order stiffness constant C turned out to be 36.06 (37.49) eV/Å^4 and 31.64 (33.21) eV/Å^4 at LT and HT from total energy (force) calculation. The higher stiffness of the lattice at LT compared to that at HT is according to expectation. Considering the Ru-O bond length differences between LT and HT at Ru1 and Ru2 octahedra, this gives rise to only a small restoring force of about 2 meV, indicating a substantial net gain driven by covalency, upon charge disproportionation created by two unequally sized octahedra.

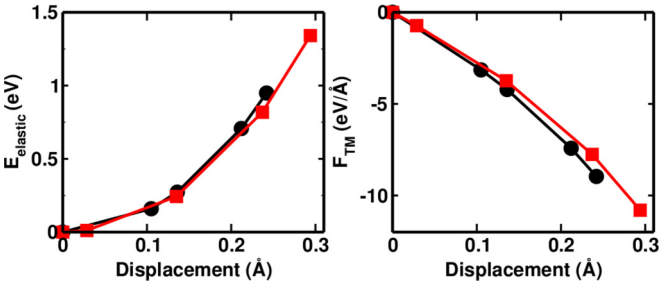

FIG. 5. (Color online) The elastic energy (left panel) and force acting on Ru ion (right panel) plotted as a function of off centric displacement, obtained from DFT calculations. The circles and squares correspond to data corresponding to HT and LT phase, respectively. For the forces in LT phase, only data corresponding to Ru1 ion has been shown, as data for Ru2 is very similar.

VI. LOW TEMPERATURE MAGNETIC STRUCTURE

The antiferromagnetic interaction between the Ru ions gives rise to a fully frustrated situation in HT. The inequivalence of Ru1 and Ru2 in Ru_4 tetrahedra in LT structure lifts this frustration only partially. This can lead to noncollinearity in the ordered magnetic structure of the Ru spins at low temperature. Possible low temperature magnetic structures have been discussed in literature [11] following the NMR results. Two different magnetic structures have been proposed, one following the consideration of zero total hyperfine field, shown in Fig. 7(b) in Ref. [11], and another following the requirement of vanishing of hyperfine field at central Hg site to be zero, shown in Fig. 7(c) in Ref. [11]. The later magnetic structure, however, was not consistent with the HT crystal structure in the sense of requirement of two inequivalent Hg sites. The LT crystal structure was not resolved during the publication of NMR results. The proposed LT trigonal structure indeed has two inequivalent Hg sites, making the magnetic structure in Fig. 7(c) of Ref. [11] to be consistent. We carried out total energy calculations of different magnetic structures on the optimized LT crystal structure, assuming both collinear and noncollinear spin arrangements as suggested in Ref. [11]. The considered magnetic structures are shown in Fig. 6. For collinear spin structure, all possible energetically distinct magnetic structures within the trigonal unit cell were considered. For the noncollinear calculations, a supercell of $2 \times 2 \times 1$ was constructed to take into account the magnetic structure proposed in Fig. 7(b) in Ref. [11]. The results of

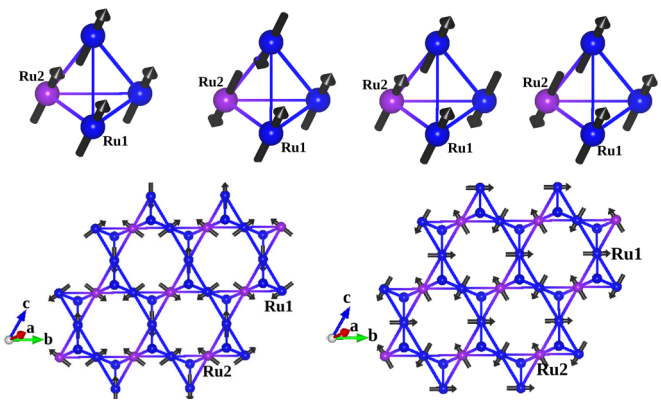

FIG. 6. (Color online) The various collinear (upper panels) and noncollinear magnetic configurations (lower panels) of Ru ions considered for total energy calculations. The noncollinear structures shown in left and right lower panels are the same as that shown in Figs. 7(b) and 7(c) in Ref. [11], respectively, and referred to as Conf.b and Conf.c in Table V.

TABLE V. Total energies for different magnetic configurations of Ru1 and Ru2 spins in optimized low temperature structure of HRO. The three Ru1 ions are labeled as 1, 2, and 3, and Ru2 is labeled as 4. Total energies (ΔE) are measured with respect to ferromagnetic configurations (FM). The other configurations are AFM1, AFM2, AFM3, and two noncollinear configurations (referred to as Conf.b and Conf.c), as shown in Fig. 6. In addition to magnetic solutions, the energy of the nonmagnetic (NM) solution is also listed.

	1	2	3	4	ΔE eV/f.u.
NM					0.101
FM					0.000
AFM1	+	+	−	−	−0.171
AFM2	+	−	+	+	−0.137
AFM3	+	+	+	−	−0.183
Conf.b					0.029
Conf.c					−0.553

calculations on collinear structures (cf. Table V) unambiguously show the dominance of antiferromagnetic interaction in general. It further shows stronger antiferromagnetic interaction between nearest neighbor Ru1 and Ru2 ions, compared to those connecting two Ru1 ions. We find there is a significant energy gain in attaining the noncollinear structure as proposed in Fig. 7(c) in Ref. [11], making it the lowest energy magnetic structure among all the considered structures.

VII. SUMMARY

To summarize, we studied the low temperature crystal structure and the corresponding electronic structure of 4*d* pyrochlore compound $Hg_2Ru_2O_7$. $Hg_2Ru_2O_7$, with unusual d^{5+} valence of Ru ion, shows first order MIT at a temperature of ≈107 K. The situation is apparently similar to that in isostructural compound $Tl_2Ru_2O_7$ with d^{4+} valence of Ru ion, which also shows a first order MIT. The MIT in $Tl_2Ru_2O_7$ is argued to be driven by the formation of orbital-ordering-assisted one-dimensional Haldane chains. The orbital ordering also drives the structural transition from cubic to orthorhombic. The nature of MIT in $Hg_2Ru_2O_7$ though is different which arises due to antiferromagnetic ordering of Ru moments. The difference arises primarily due to two reasons. Firstly, the Ru^{5+} ions in HRO are not orbitally active as Ru^{4+} ions. Secondly, the NMR experiment [11] as well as a previous DFT study [12] point towards weaker correlation effect and stronger covalency effect in HRO compared to $Tl_2Ru_2O_7$, driven by Hg *d*-Ru *d* hybridization, thus making the strong correlation driven spin-singlet formation improbable. The question remains what is then the cause and nature of structural transition observed in HRO. Our first-principles calculated low temperature crystal structure of $Hg_2Ru_2O_7$ based on experimentally proposed symmetries [13,14] shows the presence of two inequivalent RuO_6 octahedra, one which is smaller in volume and more regular (Ru2), and another which is larger in volume and more distorted (Ru1), suggestive of a charge disproportionated situation. The calculated magnetic moments at the two Ru sites, as well as the mean energy positions of two Ru t_{2g} levels, support the picture of a net charge flow from Ru2 to Ru1. The charge disproportionation is partially due to the strong covalency effect. Our study further unravels the microscopic mechanism driving the charge disproportion which turns out to be the winning of hybridization energy gain over the elastic energy loss. This charge disproportionation provides the means for Ru valence to deviate from the unusual valence of 5+, leading to observed structural distortion. The low symmetry phase in low temperature allows for two inequivalent Hg sites making the noncollinear magnetic structure as proposed in NMR study to be consistent. This results in concomitant occurrence of magnetic ordering as the primarily responsible factor for driving the MIT and the structural phase transition. Our theoretical study should motivate further experimental investigation to probe the signature of charge disproportionation.

ACKNOWLEDGMENTS

S.B. and T.S.D. thank H. Takagi for the discussion and sharing the crystal structure data. T.S.D. thanks the Department of Science and Technology (DST) for funding.

APPENDIX

TABLE VI. The hopping integral (in units of eV) t_{pd} between three different *p* orbitals of oxygen and three t_{2g} orbitals of Ru ions, the charge transfer energy (in units of eV), i.e., the onsite energy difference between the *p* and t_{2g} energy levels, as given by NMTO downfolding. Shown are the values for the Ru-O interaction in the HT phase, and Ru1-O and Ru2-O in the LT phase. Up and Dn refer to contributions in majority and minority spin channels. For the LT phase, the interactions to only oxygen atoms connecting Ru1 and Ru2 are considered. The interaction along a specific direction is shown; those in other directions can be obtained through permutation. The distortion in LT $Ru1O_6$ octahedra causes small splitting within the t_{2g} manifold, resulting in small differences in charge transfer energy of the t_{2g} orbitals from a specific *p* orbital, which is shown by the numbers within brackets.

Connecting vector			Hopping integral (t_{pd})			Charge transfer energy	
			p_1	p_2	p_3		($\lvert\Delta_{pd}\rvert$)
HT(Ru-O)	Up	t_{2g1}	−0.321	0.575	0.675	$\Delta_{p1,d}$	4.104
		t_{2g2}	0.675	0.600	−0.321	$\Delta_{p2,d}$	2.106
		t_{2g3}	0.002	−0.072	0.003	$\Delta_{p3,d}$	2.441
	[0.125 0.125 − 0.071]		p_1	p_2	p_3		
	Dn	t_{2g1}	−0.329	0.599	0.725	$\Delta_{p1,d}$	7.127
		t_{2g2}	0.725	0.600	−0.329	$\Delta_{p2,d}$	4.974
		t_{2g3}	0.005	−0.067	0.006	$\Delta_{p3,d}$	5.464

TABLE VI. (*Continued*.)

Connecting vector			Hopping integral (t_{pd})				Charge transfer energy
			p_1	p_2	p_3		($\lvert\Delta_{pd}\rvert$)
LT(Ru1-O)	Up	[−0.115 0.000 − 0.448]	t_{2g1}	−0.463	−0.175	0.000	$\Delta_{p1,d}$ 2.167 (2.365)
			t_{2g2}	0.721	0.395	0.000	$\Delta_{p2,d}$ 3.865 (4.063)
			t_{2g3}	0.000	0.000	−1.025	$\Delta_{p3,d}$ 1.787 (1.985)
				p_1	p_2	p_3	
	Dn		t_{2g1}	−0.483	−0.196	0.000	$\Delta_{p1,d}$ 5.198 (5.484)
			t_{2g2}	0.739	0.389	0.000	$\Delta_{p2,d}$ 6.710 (6.996)
			t_{2g3}	0.000	0.000	−1.116	$\Delta_{p3,d}$ 4.809 (5.095)
LT(Ru2-O)	Up	[0.385 0.000 0.260]		p_1	p_2	p_3	
			t_{2g1}	0.000	−0.032	0.053	$\Delta_{p1,d}$ 3.933
			t_{2g2}	−0.772	−0.516	0.313	$\Delta_{p2,d}$ 5.632
			t_{2g3}	−0.772	0.516	−0.313	$\Delta_{p3,d}$ 3.554
				p_1	p_2	p_3	
	Dn		t_{2g1}	0.000	−0.021	0.042	$\Delta_{p1,d}$ 2.661
			t_{2g2}	−0.755	−0.545	0.366	$\Delta_{p2,d}$ 4.173
			t_{2g3}	−0.755	0.545	−0.366	$\Delta_{p3,d}$ 2.272

[1] M. J. Harris, S. T. Bramwell, D. F. McMorrow, T. Zeiske, and K. W. Godfrey, Phys. Rev. Lett. **79**, 2554 (1997).

[2] M. A. Subramanian, G. Aravamudan, and G. V. Subba Rao, Prog. Solid State Chem. **15**, 55 (1983).

[3] F. Ishii and T. Oguchi, J. Phys. Soc. Jpn. **69**, 526 (2000).

[4] H. Sakai, M. Kato, K. Yoshimura, and K. Kosuge, J. Phys. Soc. Jpn. **71**, 422 (2002).

[5] Hironori Sakaia, Kazuyoshi Yoshimura, Harukazu Kato, Shinsaku Kambe, and Russell E. Walstedt, J. Phys. Chem. Solids **63**, 1039 (2002).

[6] N. Taira, M. Wakeshima, and Y. Hinatsu, J. Phys.: Condens. Matter **11**, 6983 (1999).

[7] R. Wang and A. W. Sleight, Mater. Res. Bull. **33**, 1005 (1998); T. Munenaka and H. Sato, J. Phys. Soc. Jpn. **75**, 103801 (2006).

[8] W. Klein, R. Kremer, and M. Jansen, J. Mater. Chem. **17**, 1356 (2007).

[9] N. Takeshita, C. Terakura, Y. Tokura, A. Yamamoto, and H. Takagi, J. Phys. Soc. Jpn. **76**, 063707 (2007); A. Yamamoto, P. A. Sharma, Y. Okamoto, A. Nakao, H. A. Katori, S. Niitaka, D. Hashizume, and H. Takagi, *ibid.* **76**, 043703 (2007).

[10] S. Lee, J. G. Park, D. T. Adroja, D. Khomskii, S. Streltsov, K. A. Mcewen, H. Sakai, K. Yoshimura, V. I. Anisimov, D. Mori, R. Kanno, and R. Ibberson, Nat. Mater. **5**, 471 (2006).

[11] M. Yoshida, M. Takigawa, A. Yamamoto, and H. Takagi, J. Phys. Soc. Jpn. **80**, 034705 (2011).

[12] Santu Baidya, Soumyajit Sarkar, T. Saha-Dasgupta, and D. D. Sarma, Phys. Rev. B **86**, 125117 (2012)

[13] J. van Duijn, R. Ruiz-Bustos, and A. Daoud-Aladine, Phys. Rev. B **86**, 214111 (2012).

[14] H. Takagi *et al.* (unpublished).

[15] S. Kawasaki, M. Takano, R. Kanno, T. Takeda, and A. Fujimori, J. Phys. Soc. Jpn. **67**, 1529 (1998); P. M. Woodward, D. E. Cox, E. Moshopoulou, A. W. Sleight, and S. Morimoto, Phys. Rev. B **62**, 844 (2000).

[16] M.-H. Whangbo, H.-J. Koo, A. Villesuzanne, and M. Pouchard, Inorganic Chemistry **41**, 1920 (2002).

[17] P. Blaha, K. Schwartz, G. K. H. Madsen, D. Kvasnicka, and J. Luitz, *WIEN2K, An Augmented Plane Wave + Local Orbitals Program for Calculating Crystal Properties*, edited by K. Schwarz (Technische Universitaët Wien, Austria, 2001).

[18] G. Kresse and J. Furthmüller, Phys. Rev. B **54**, 11169 (1996).

[19] O. K. Andersen and O. Jepsen, Phys. Rev. Lett. **53**, 2571 (1984).

[20] O. K. Andersen and T. Saha-Dasgupta, Phys. Rev. B **62**, R16219(R) (2000).

[21] P. E. Blöchl, O. Jepsen, and O. K. Andersen, Phys Rev B **49**, 16223 (1994).

[22] P. E. Blöchl, Phys. Rev. B **50**, 17953 (1994).

[23] J. P. Perdew, K. Burke, and M. Ernzerhof, Phys. Rev. Lett. **77**, 3865 (1996).

[24] V. I. Anisimov, I. V. Solovyev, M. A. Korotin, and G. A. Sawatzky, Phys. Rev. B **48**, 16929 (1993).

[25] R. F. W. Bader, *Atoms in Molecules: A Quantum Theory* (Oxford University Press, New York, 1990).

[26] W. Luo, A. Franceschetti, M. Varela, J. Tao, S. J. Pennycook, and S. T. Pantelides, Phys. Rev. Lett. **99**, 036402 (2007).

[27] H. Raebiger, S. Lany, and A. Zunger, Nature (London) **453**, 763 (2008).

[28] H. Park, A. J. Millis, and C. A. Marianetti, Phys. Rev. Lett. **109**, 156402 (2012).

[29] D. I. Khomskii, J. Magn. Magn. Mater. **306**, 1 (2006).